Journal of Chemistry and Technologies, 2023, *31*(3), 477-485

Journal of Chemistry and Technologies

pISSN 2663-2934 (Print), ISSN 2663-2942 (Online).

journal homepage: http://chemistry.dnu.dp.ua

UDC 546.05 + 546.06

THEORETICAL STUDY OF THE PHOSPHATE UNITS STABILITY BY THE DFT B3LYP/6-311G QUANTUM METHOD

A. El Addali[1*], A. El Boukili[2], L. Boudad[2], M. Taibi[2], T. Guedira[1]

[1] Ibn Tofail University in Kenitra, Laboratory of Organic Chemistry, Catalysis and Environment, (LOCCE), Faculty of Sciences, Kenitra, Morocco

[2] Mohammed V University in Rabat, Centre Sciences des Matériaux, Laboratoire de Physico-Chimie des Matériaux Inorganiques et Organiques (LPCMIO), Ecole Normale Supérieure (E.N.S), Rabat, Morocco

Received 3 August 2023; accepted 7 September 2023; available online 25 October 2023

Abstract

The phosphate units have been theoretically investigated through density functional theory (DFT) calculations. Ionization potential (I), electron affinity (A), electrophilicity index (ω), chemical potential (μ), hardness (η), softness (S), and dipole moment (P) have been optimized. The obtained results revealed that the $[PO_4]^{3-}$ (Q_0) units act as electron donors, while the $[P_4O_{10}]^0$ (Q_3) unit acts as an electron acceptor. The passage from one unit to the other implies an increase in the number of bridging oxygens (BO) consistent with the variation of Mulliken charges. Moreover, the analysis of the optimized contours of the electrostatic potential has indicated that the electrophilic attack is more expected on the P-O-P bonds. The infrared and Raman spectra have been also predicted and the change of symmetric and asymmetric vibrational bands of the phosphate units with the number of bridging oxygens has been investigated.

Keywords: DFT; electrophilic; electrostatic potential; Global reactivity indices; phosphate units.

ТЕОРЕТИЧНЕ ДОСЛІДЖЕННЯ СТАБІЛЬНОСТІ ФОСФАТНИХ СПОЛУК КВАНТОВИМ МЕТОДОМ DFT B3LYP/6-311G

А. Ель Аддалі[1*], А. Ель Букілі[2], Л. Будад[2], М. Тайбі[2], Т. Гедіра[1]

[1]Університет Ібн Тофаїла в Кенітрі, Лабораторія органічної хімії, каталізу та навколишнього середовища (LOCCE), факультет природничих наук, Кенітра, Марокко.

[2]Університет Мохаммеда V в Рабаті, Центр наук про матеріали, Лабораторія фізико-хімії неорганічних і органічних матеріалів (LPCMIO), Вища нормальна школа (E.N.S.), Рабат, Марокко.

Анотація

Фосфатні агрегати були теоретично досліджені за допомогою розрахунків теорії функціоналу густини (DFT). Оптимізовано потенціал іонізації (I), спорідненість до електрона (A), індекс електрофільності (ω), хімічний потенціал (μ), твердість (η), м'якість (S) та дипольний момент (P). Отримані результати показали, що агрегати $[PO_4]^{3-}$ (Q_0) діють як донори електронів, в той час як агрегат $[P_4O_{10}]^0$ (Q_3) діє як акцептор електронів. Перехід від одних одиниць до інших передбачає збільшення кількості місткових оксигенів (МО), що відповідає зміні заряду Маллікена. Крім того, аналіз оптимізованих контурів електростатичного потенціалу показав, що електрофільна атака є більш очікуваною на зв'язках P-O-P. Також спрогнозовано ІЧ та раманівські спектри і досліджено зміну симетричних та асиметричних коливальних смуг фосфатних одиниць залежно від кількості місткових оксигенів.

Ключові слова: DFT; електрофільність; електростатичний потенціал; індекси глобальної реакційної здатности; фосфатні одиниці.

**Corresponding author: e-mail: hioaddali@gmail.com*

doi: 10.15421/jchemtech.v31i3.285545

Introduction

Owing to their interesting combination of physical and chemical properties, phosphates glasses have drawn a growing interest over the last decades. These glasses are produced by melting a large variety of alkali metal oxides, transition metal oxides, alkaline oxides, and rare-earth oxides with phosphorus. Compared to other inorganic glasses families, phosphate glasses exhibit higher electrical conductivity, lower transition temperature, and higher thermal expansion coefficients relative to silicate and borate glasses. These features make them potential candidates for a wide range of technological applications such as sensors [1], data storage [2], solid-state batteries [3], and laser technologies [4].

Phosphate glasses are materials with a structure formed by phosphate tetrahedrons PO_4 that fit together by forming bonds between each other. This class of glasses can also be described, according to [5], as a three-dimensional cross-linked network of phosphate tetrahedra denoted Qi, where i refers to the number of neighboring tetrahedra linked through a common oxygen bridge [6; 7].

They are four possible structural entities of the PO_4 tetrahedron, which are denoted as follows:

- Q_0: ($[PO_4]^{3-}$) : The unit Q_0 consists of four oxygens that are non-bridging (NBO).
- Q_1: ($[P_2O_7]^{4-}$) : Two $[PO_4]$ tetrahedra are linked together by a common oxygen atom, which acts as a bridging oxygen (BO) forming a ($[P_2O_7]^{4-}$) molecule.
- Q_2: ($[P_3O_9]^{3-}$) : Three $[PO_4]$ tetrahedra are connected through oxygen bridges to form the $[P_3O_9]^{3-}$ structural entity.
- Q_3: ($[P_4O_{10}]^0$: Four $[PO_4]$ tetrahedra are connected through oxygen bridges to create the $[P_4O_{10}]^0$ structural unit.

These units are the main elements forming the lattice of phosphate glasses, and the more they, together with other forming and modifying oxides, participate in the development of these lattices, the greater their interest in the chemical and optical fields. [8; 9].

The purpose of this paper is to study the phosphate units through the DFT calculation method using the B3LYP function associated with the 6-311G base [10–13]. The chemical reactivity of these units has been interpreted using the global reactivity indices. HOMO-LUMO energy gaps, ionization potential (I), electron affinity (A), electrophilicity index (ω), chemical potential (μ), hardness (ŋ), and softness (S) are investigated. This paper reports also on the determination of charges, dipole moments, and optimized contours of the molecular electrostatic potential. The vibrational modes of these units are also explored via the simulated IR and Raman spectra.

Computational details. All the reported calculations were conducted using the Gaussian 09 software program, based on the DFT/RB3LYP density functional theory method with a 6-311G basis set [11]. The stability of phosphate units was optimized with respect to charges, EHOMO and ELUMO molecular orbital energies, electrostatic potentials, and global reactivity indices. The equilibrium structure was achieved with the absence of imaginary frequencies.

The ionization energy or ionization potential (IP), defined as the minimum energy required to extract an electron from an atom or molecule, has been calculated by the following relationship:

$$\mathrm{IP} = -\mathrm{E_{HOMO}} \qquad (1)$$

The electron affinity (EA) denoting the released energy due to the capture of an electron has been estimated via the following relation:

$$\mathrm{AE} = -\mathrm{E_{LUMO}} \qquad (2)$$

The chemical potential is a parameter associated with electrophilicity (attraction of electrons) and nucleophilicity (release of electrons). This chemical potential is calculated as follows [14; 15].

$$\mu = \frac{-(IP + AE)}{2} \qquad (3)$$

The chemical hardness (η) is a parameter that is also reflective of the stability of a molecular system. It provides the resistance to electron transfer (charge transfer), whether electron gain or loss. The chemical hardness has been calculated via the equation [14; 16].

$$\eta = \frac{IP - AE}{2} \qquad (4)$$

The overall electrophile index (ω) is defined as the ability of a molecular system to bind strongly to a nucleophilic partner via electron transfer. The higher the value of ω, the more electrophilic the system is. The overall electrophile index is given by [15; 16].

$$\omega = \frac{\mu^2}{2\eta} \qquad (5)$$

Besides the dipole moment (P) measuring the polarity of the molecule, the softness (S) representing the ability of an atom or molecule to hold a charge was calculated according to the formula [14; 15].

$$\mathrm{S} = \frac{1}{\eta} \qquad (6)$$

Journal of Chemistry and Technologies, 2023, *31*(3), 477-485

Results and discussion

*The geometry optimization.*The geometry optimization of isolated phosphate units with their charges is illustrated in figure 1. The optimization process was carried out using monomer wave functions at the B3LYP/6-311G level. The optimization procedure involved visual observations and sets approximation in the gaussian 09 w software. the resulting structural parameters are presented in table 1.

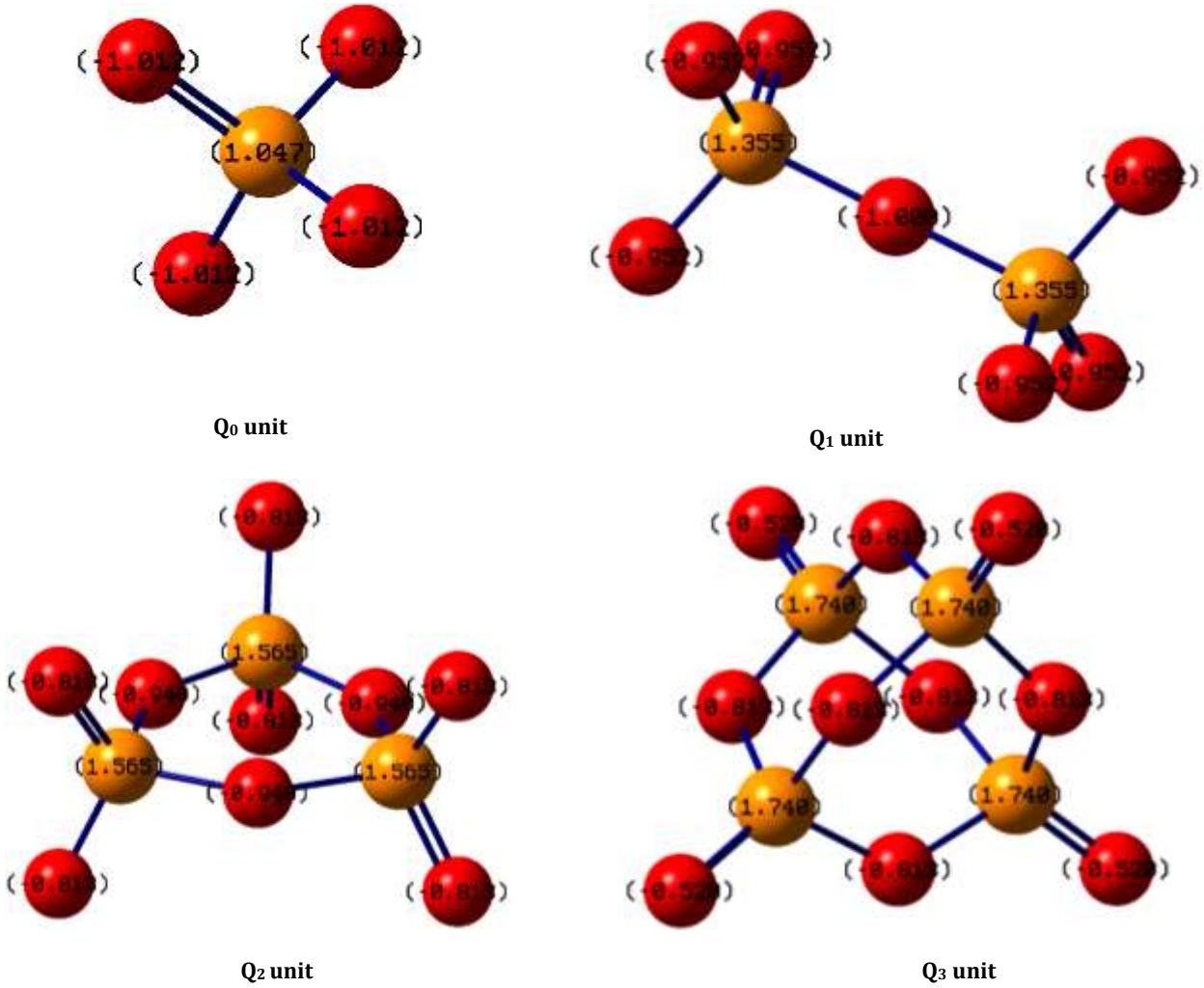

Fig. 1. Mulliken charges of the optimized Q_0, Q_1, Q_2, and Q_3 units with the program GAUSSIAN 09W/B3LYP-6-311G."

Table 1

Calculated interatomic distances and angles of the Q_0, Q_1, Q_2 and Q_3 phosphate units for the optimized structures.

		Q_0	Q_1	Q_2	Q_3
Lengths (Å) (±0.001Å)	$P-O_{NBO}$	1.688	1.651	1.597	1.536
	$P-O_{BO}$	----------	1.781	1.740	1.724
Angles (°) (±0.001°)	$P-O-P$	----------	179.750	140.580	126.850
	$O_{NBO}-P-O_{NBO}$	109.470	111.510	118.330	----------
	$O_{NBO}-P-O_{BO}$	----------	107.350	109.200	118.160
	$O_{BO}-P-O_{BO}$	----------	----------	99.380	99.550

One can observe that increasing the number of bridging oxygen atoms and transitioning between units results in an increase in positive charges on the phosphorus atoms and negative charges on the oxygen atoms. Bridging oxygens (BO) are involved in forming bridges between different units, while non-bridging oxygens (NBO) do not participate in such bridging interactions. The electron density of positive charges is concentrated on the phosphorus atom, while the negative charges are concentrated on the oxygen atoms BO and NBO. Moreover, the phosphorus cation P^{5+} is placed in the middle of the almost perfect tetrahedron with an angle O - P - O of 109.47° very close to the ideal value (109.5°). For the Q_1 structural unit, it can be noticed that the P-O_{BO} bond length has a value of 1.781Å higher than the P-O_{NBO} one having a value of 1.651 Å. Also, the

two phosphorus atoms and the bridging oxygen are found to be aligned as the two neighboring tetrahedra are connected at an angle of 179.75°. Furthermore, the tetrahedral angle O_{NBO}-P-O_{NBO} is about 111.51°, higher than that of Q_0 where the angle is 109.47°. This implies a higher tetrahedral distortion due to the P-O_{BO} bond elongation. For the $[P_3O_9]^{3-}$ unit with Q_2 notation, the tetrahedra are connected through two bridging oxygens, with P-O_{NBO} and P-O_{BO} distances of 1.597 Å and 1.740 Å, respectively. Besides, the value of the P-O-P angle is revealed to be about 140.58° reflecting the onset of further decrease of this angle. Furthermore, one observes an increase in the value of the O_{NBO}-P-O_{NBO} angle to about 118.33° owing to the distortion of the $[PO_4]$ tetrahedra. For the Q_3 unit, the P-O_{NBO} and P-O_{BO} distances decline and reach values of 1.536Å and 1.724Å, respectively. Further, the tetrahedra are found to be connected at an average angle of 99.55°, which seems to be far from the equilibrium geometry.

Molecular electrostatic potential (MESP). The molecular electrostatic potential (MESP) is a valuable tool that offers insights into the size and overall shape of a molecule [17]. It is commonly used to study the electrostatic interactions within a chemical system. In the MESP map, the different values of the electrostatic potential contour are represented by different colors. The most negative electrostatic potential region is illustrated by red color, the most positive electrostatic potential region is represented by green color. [18].

The partial atomic charge and local reactivity descriptors highlight the reactive sites of the molecule and provide insight into its reactivity. Figure 2 reveals that the molecular electrostatic potential is centered on the P-O-P bonds for the three phosphate units Q_1, Q_2, and Q_3, whereas it is centered on the phosphorus atom for the Q_0 unit. These findings point to the planar applicability of this parameter and thus imply that the attack of an electrophile is more likely to occur on the P-O-P bonds. On the other hand, Figure 2 confirms that the density of positive charges is concentrated on the phosphorus atom.

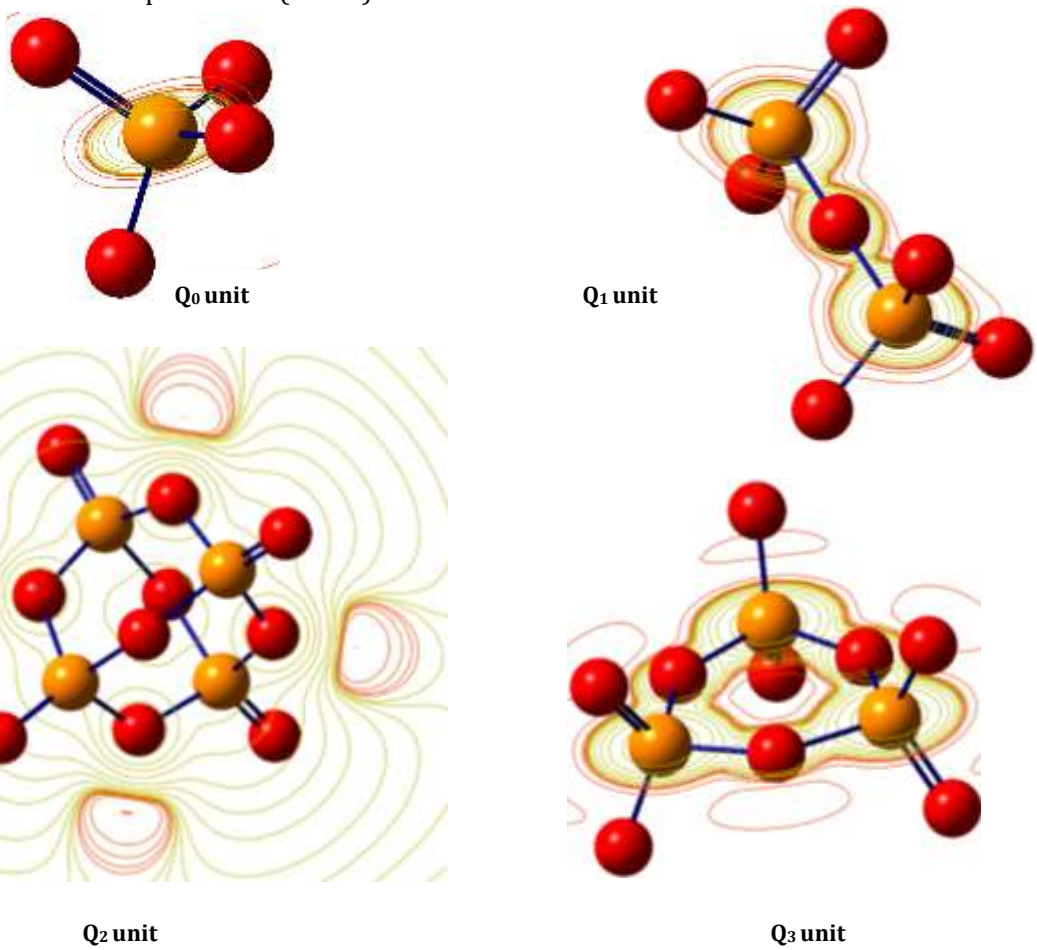

Fig. 2. The electrostatic potential (ESP) of the different optimized units with the program GAUSSIAN 09W/B3LYP-6-311G."

Study of global reactivity. The frontier molecular orbitals (FMOs) are also used to describe the interactions of units with the other molecules [19]. These orbitals are the major aspect that tells us about the stability of the phosphate units.

Table 2 groups the computed values of HOMO and LUMO energies, energy difference ΔE, chemical potential, softness, chemical hardness, overall electrophilic number, and dipole moment for the different studied phosphate units. The obtained results indicate that the Q_0 units display a greater energy difference of 7.831968 eV compared to the Q_1 units. Additionally, the Q_0 units exhibit a low softness value of 0.25536 eV and a higher overall electrophile index of 26.14391eV, in contrast to the Q_1 unit.

The Q_0 unit exhibits a higher chemical potential μ of 14.309376 eV, along with a greater electrophilicity index ω of 26.14391 eV. These characteristics indicate that there is a propensity for electron transfer from Q_0 to another molecule, classifying Q_0 as an electron donor. However, the lower energy difference and the larger softness factor of the Q_3 units indicate an electron acceptor. The chemical hardness η of the Q_3 unit (η_{Q3} = 2,7413 eV) is lower than that of the other units, implying that this unit represents a less resistance to accept or give electronic charges compared to the Q_0, Q_1, and Q_2 units.

Table 2

HOMO and LUMO energies, energy difference ΔE, chemical potential, softness, chemical hardnes, overall electrophile index, and dipole moment.

Unit	E_{HOMO} (eV)	E_{LUMO} (eV)	ΔE(eV)	η (eV)	S (eV^{-1})	μ (eV)	ω (eV)	P (D)
Q_0	10.39339	18.22536	7.83196	3.91598	0.25536	14.30937	26.14391	0.0000
Q_1	10.59385	16.46252	5.86867	2.93433	0.34079	13.52819	31.18456	0.0020
Q_2	4.00030	9.95084	5.95054	2.97527	0.33610	6.97557	8.17718	0.0009
Q_3	-10.82451	-5.34180	5.48270	2.74135	0,36478	7.34180	9.83131	0.0000

However, the zero value of the dipole moment of the Q_0 and Q_3 units indicates the presence of a symmetry element in these units. Meanwhile, the higher dipole moment of the Q_1 unit is found to be 0.0020, implying the non-coincidence of the negative and positive charge barycenters and thus the polarity of this unit.

The HOMO-LUMO gap is a crucial factor in quantum chemistry as it enables the study of unit stability [20,21]. The unit phosphate Q_3 exhibits a very low HOMO-LUMO energy gap of 5.48270 eV, which results in a strong bond formation with other polarizable molecules. This highly desirable property facilitates potential intermolecular interactions between the units of phosphate and other units. However, from the value of E_{HOMO} we can determine the electron-donating ability, and from the value of E_{LUMO} we find the electron-accepting ability. In conjugated systems (Q_1, Q_2, Q_3), there is a slight difference between HOMO–LUMO, due to which electron (charge) can transfer from one atom (electron donor groups) to the other (e-accepting groups) via a pi-conjugated system [22], In this context and based on the obtained results (Table 3), one can observe that the Q_0 units behave as electron donors whereas the Q_3 ones are electron acceptors.

Table 3

Energy differences in eV (error ±0.00027) between the various HOMO/LUMO combinations of reactants.

$E_{HOMOQ_0} - E_{LUMOQ_1}$	$E_{HOMOQ_1} - E_{LUMOQ_0}$	$E_{HOMOQ_2} - E_{LUMOQ_0}$	$E_{HOMOQ_3} - E_{LUMOQ_0}$
6.06861	7.63151	14.22506	29.04987
$E_{HOMOQ_0} - E_{LUMOQ_2}$	$E_{HOMOQ_1} - E_{LUMOQ_2}$	$E_{HOMOQ_2} - E_{LUMOQ_1}$	$E_{HOMOQ_3} - E_{LUMOQ_1}$
0.44255	0.64301	12.46222	27.28703
$E_{HOMOQ_0} - E_{LUMOQ_3}$	$E_{HOMOQ_1} - E_{LUMOQ_3}$	$E_{HOMOQ_2} - E_{LUMOQ_3}$	$E_{HOMOQ_3} - E_{LUMOQ_2}$
15.73519	15.93566	9.34210	20.77535

Spectroscopic study. The optimized geometries of the studied phosphate units were employed to compute their theoretical FTIR and RAMAN spectra. The obtained spectra are presented in Figure 3a-b and the corresponding frequencies of the different bands and their assignments are summarized in Table 4. It is important to note that DFT calculations are known to produce a shifting of experimental frequencies with a scaling factor of approximately 0.965 - a common correction applied to DFT-calculated frequencies to bring them into better agreement with experimental values for the B3LYP functional with the basis set 6-311G.

Analyzing the calculated FTIR spectrum of the isolated structural unit Q_0 (Figure 3a) is composed of two bands. The lower frequency band at 456

cm^{-1} results from the symmetrical deformation vibrations of the

O-P-O angles. Besides, the strongest band centered at about 821 cm^{-1} is due to asymmetric stretching vibrations of P-O bonds. Although the same features are also noticed in the Raman spectrum (Figure 3b), there are two additional active modes of high intensity at 316 cm^{-1} and 658 cm^{-1}, which can be attributed to the symmetric deformation vibrations of the O-P-O angle and the symmetric stretching vibrations of the P-O bonds.

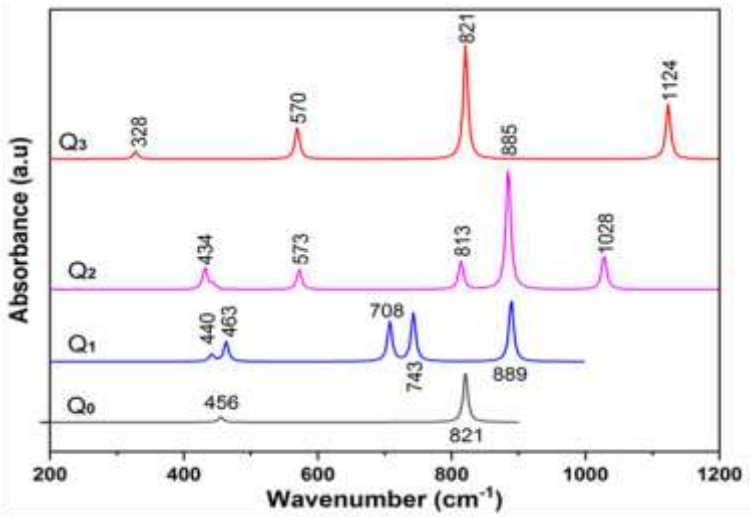

Fig. 3a. Calculated FTIIR spectra of simulated Q_0, Q_1, Q_2 and Q_3 phosphate units.

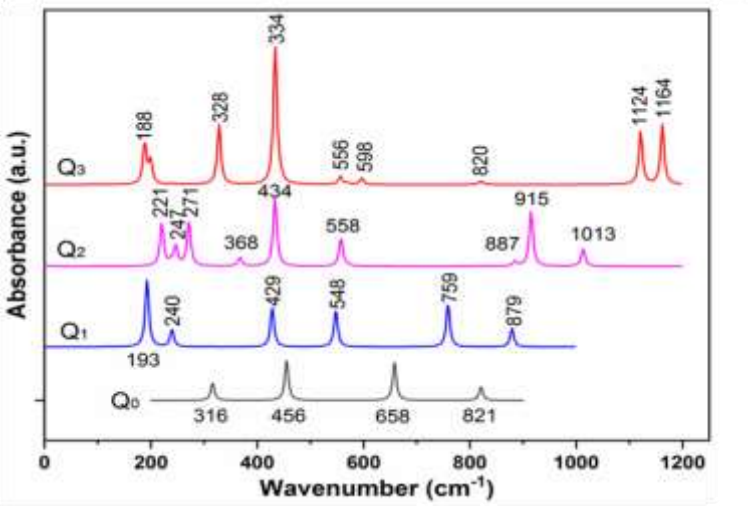

Fig. 3b. Calculated Raman spectra of simulated Q_0, Q_1, Q_2 and Q_3 phosphate units.

The FTIR spectrum of the Q_1 unit shows five characteristic bands. The band located around 708 cm^{-1}, and 743 cm^{-1} are associated with the asymmetric stretching vibrations of P-O-P bonds, and symmetric stretching vibrations of P-O bonds in Q_1 tetrahedra, respectively. Moreover, the strong band at 889 cm^{-1} is related to the asymmetric stretching vibrations of P-O bonds. These vibrational modes were also detected via Raman spectroscopy. Indeed, the peaks appearing at 193 cm^{-1}, 429 cm^{-1}, 548 cm^{-1}, and 759 cm^{-1} correspond to symmetric stretching vibrations of P-O-P bonds, symmetric stretching vibrations of O-P-O bonds, as well as symmetric and asymmetric stretching vibrations of P-O bonds in Q_1 tetrahedra, respectively. However, the Q_2 phosphate unity infrared spectrum is found to be composed of five characteristic bands centered at about 434 cm^{-1}, 573 cm^{-1}, 814 cm^{-1}, 885 cm^{-1}, 1028 cm^{-1} and associated with the symmetric deformation of O–P–O angles as well as symmetric and asymmetric stretching vibrations of P–O–P and P–O bonds. Meanwhile, the Raman spectrum in the Q_2 unit showed different vibrational modes corresponding to symmetric deformation vibrations of the O-P-O angles, symmetric stretching vibrations of P-O-P bands, as well as asymmetric and symmetric stretching vibrations of the P-O bonds in the Q_2 tetrahedra. For the three-dimensional Q_3 units, the intense peak at

821 cm^{-1} is related to the asymmetric stretching vibrations of P–O–P bonds. The two peaks at 570 cm^{-1} and 1124 cm^{-1} reflect the asymmetric vibrations of the O–P–O angles and the P–O bonds, respectively. Besides, the weak peak at 328 cm^{-1} is associated in turn with the symmetric deformation of the O–P–O angles. However, the Raman spectrum shows six vibration modes located at 188 cm^{-1}, 328 cm^{-1}, 434 cm^{-1}, 556 cm^{-1}, 1124 cm^{-1}, and 1164 cm^{-1}. These correspond to the symmetric deformation vibrations of the O–P–O angles and the stretching vibrations of P–O bonds in the phosphate tetrahedra. All these detected vibrational modes for the Q_0, Q_1, Q_2, and Q_3 units have been detected for the Q_3 unit through further IR and Raman bands as summarized in Table 4.

Table 4

Calculated IR and Raman active modes and frequency assignment for structural units of phosphate (v.w – very weak, f – weak, m – medium, s – strong, v.s – very strong)

Wavenumbers (cm^{-1})	IR	Raman	Assignement
			Q_0
316	-	m	Symmetric deformation vibrations of angles O–P–O [23; 24].
456	v.w	v.s	Symmetric deformation vibrations of angles O–P–O [23; 24].
658	-	v.s	Symmetric stretching vibrations of P–O bonds [23; 24].
821	v.s	m	Asymmetric stretching vibrations of P–O bonds [23; 24].
			Q_1
193	-	v.s	Symmetric stretching vibrations of P–O bonds [25].
240	-	m	Symmetrical deformation vibrations of angles O – P – O in Q_1 tetrahedra [26; 27].
429	-	s	Symmetrical deformation vibrations of angles O – P – O in Q_1 tetrahedra [26; 27].
445	w	-	Symmetrical deformation vibrations of angles O – P – O in Q_1 tetrahedra, symmetric deformation vibrations of the angle P – O – P [26; 27; 28].
464	m	-	Asymmetrical deformation vibrations of angles O – P – O in Q_1 tetrahedra [26,27].
548	-	s	Symmetric stretching vibrations of P–O–P bonds [25].
708	s	-	Asymmetric stretching vibrations of P–O–P bonds [29; 30]. Symmetric stretching vibrations of P–O bonds in Q_1 tetrahedra [28; 29].
743	s	-	Asymmetric stretching vibrations of P–O–P bonds, symmetric stretching vibrations of P–O bonds in Q_1 tetrahedra [28; 29; 30].
759	-	s	Symmetric stretching vibrations of P–O bonds in Q_1 tetrahedra, symmetric stretching vibrations of P–O–P bonds [25; 28; 29].
879	-	m	Asymmetric stretching vibrations of P–O bonds in Q_1 tetrahedra [28; 29].
889	v.s	-	Asymmetric stretching vibrations of P–O bonds in Q_1 tetrahedra [28; 29].
			Q_2
221	-	s	Symmetric deformation vibrations of O–P–O angles in Q_2 tetrahedra [26; 27].
247	-	w	Symmetric deformation vibrations of O–P–O angles in Q_2 tetrahedra [26; 27].
271	-	s	Symmetric deformation vibrations of O–P–O angles in Q_2 tetrahedra [26; 27].
368	-	v.w	Symmetric deformation vibrations of O–P–O angles in Q_2 tetrahedra [26; 27].
434	m	v.s	Symmetric deformation vibrations of O–P–O angles in Q_2 tetrahedra [26; 27].
558	-	s	Symmetric deformation vibrations of angles P–O–P [28].
573	m	-	Symmetric stretching vibrations of P–O–P bonds [25].
814	m	-	Asymmetric stretching vibrations of P–O–P bonds [29; 30]. Symmetric stretching vibrations of P–O bonds in Q_2 tetrahedra [28; 29].
885	v.s	v.w	Asymmetric stretching vibrations of P–O–P bonds [29; 30].
			Symmetric stretching vibrations of P–O bonds in Q2 tetrahedra [28; 29].
915	-	v.s	Symmetric stretching vibrations of P–O bonds in Q2 tetrahedra [28; 29].
1013	-	m	Asymmetric stretching vibrations of P–O bonds in Q_2 tetrahedra [28; 29].
1028	m	-	Symmetric stretching vibrations of P–O bonds in Q2 tetrahedra [28; 29].
			Q_3
188	-	s	Symmetric deformation vibrations of O–P–O angles in Q_2, Q_3 tetrahedra [26; 27].
208	vw	s	Symmetric deformation vibrations of O–P–O angles in Q_2, Q_3 tetrahedra [26; 27].
434	-	v.s	Symmetric deformation vibrations of O–P–O angles in Q_3 tetrahedra [26; 27].
556		vw	Symmetric deformation vibrations of O–P–O angles in Q_3 tetrahedra [26; 27].
570	-	v.w	Asymmetric deformation vibrations of O–P–O angles in Q_3 tetrahedra [26; 27].
821	w	-	Asymmetric stretching vibrations of P–O–P bonds [29; 30].
1124	-	v.s	Asymmetric stretching vibrations of P–O bonds in Q_2 tetrahedra [28; 29].
1164	w	-	Symmetric stretching vibrations of P–O bonds in Q_2 tetrahedra [28; 29].

Conclusion

Phosphate units with varied numbers of bridging oxygens (BO) were studied by theoretical calculations performed using the RB3LYP/6-311G DFT quantum method to determine the electron density, bond lengths and angles, and assess the molecular electrostatic potential. Additionally, we analyzed the chemical reactivity of these units by examining

global reactivity indices. Furthermore, we investigated the vibrational modes of these units by simulating IR and Raman spectra. Our findings have led to the following conclusions:

- Charges were observed to increase with the number of bridging oxygens (BO).

- The electrostatic potential is primarily concentrated on the phosphorus atoms and bridging oxygens (BO).

- By comparing the energy differences between the two possible combinations of HOMO/LUMO for these four units, we conclude that Q_0 unit acts as an electron donor, while Q_3 acts as an electron acceptor.

- Units Q_0 and Q_3 exhibit a zero dipole moment, whereas Q_1 has a higher dipole moment, indicating that this unit is polarizable.

- Shift bands of symmetrical and asymmetrical vibrations of Qi units were observed to vary with the number of bridging oxygens (BO).

Disclosure statement

Conflict of Interest: The authors declare that there are no conflicts of interest.

Compliance with Ethical Standards: This article does not contain any studies involving human or animal subjects.

References

[1] Chen, Y., Liu, X. Y., Chen, G. H., Yang, T., Yuan, C. L., Zhou, C. R., Xu, J. W. (2017). Up-conversion luminescence and temperature sensing characteristics of Er^{3+}/Yb^{3+} co-doped phosphate glasses, *J. Mater. Sci. Mater. Electron.*, *28*(20), 15657–15662. https://doi.org/10.1007/s10854-017-7454-9

[2] Canioni, L., Bellec, M., Royon, A., Bousquet, B., Cardinal, T. (2008). Three-dimensional optical data storage using third-harmonic generation in silver zinc phosphate glass. *Opt. Lett.*, *33*(4), 360–362. https://doi.org/10.1364/OL.33.000360

[3] Das, S.S., Baranwal, B.P., Gupta, C.P., Singh, P. (2003). Characteristics of solid-state batteries with zinc/cadmium halide-doped silver phosphate glasses as electrolytes. *J. Power Sources*, *114*(2), 346–351. https://doi.org/10.1016/S0378-7753(02)00604-3

[4] Juárez-Batalla, J., Meza-Rocha, A. N., Camarillo, I., Caldiño, U. (2016). Luminescence properties of Tb^{3+}-doped zinc phosphate glasses for green laser application. *Opt.*, *58*, 406–411. https://doi.org/10.1016/j.optmat.2016.06.022

[5] Zachariasen, W. H. (1932) The atomic arrangement in glass. *J. Am. Chem. Soc.*, *54*(10), 3841–3851. https://doi.org/10.1021/ja01349a006

[6] Brow, R. K., (2000) Review: the structure of simple phosphate glasses, *J. Non- Cryst. Solids*, *263–264*, 1–28

[7] Hoppe, U. (1996) A structural model for phosphate glasses, *J. Non-Cryst. Solids*, *195*(12), 138–147. https://doi.org/10.1016/S0022-3093(99)00620-1

[8] Abe, Y., Hayashi, M., Iwamoto, T., Sumi, H., Hench, L. (2005). Superprotonic conducting phosphate glasses containing water, *J. Non-Cryst. Solids*, 351(2426) 2138–2141. https://doi.org/10.1016/j.jnoncrysol.2005.05.010

[9] Broer, M. M., Bruce, A. J., Grodkiewicz, W. H. (1992). Photoinduced refractive-index changes in several Eu^{3+}-, Pr^{3+}-, and Er^{3+}-doped oxide glasses, *Phys. Rev. B*, *45*(13) 7077–7083. doi: 10.1103/physrevb.45.7077

[10] Lee, C., Yang, W., Parr, R. G. (1988). Development of the Colle-Salvetti correlation-energy formula into a functional of the electron density. *Phys. Rev. B*, *37*(2) 785. https://doi.org/10.1103/PhysRevB.37.785

[11] Frisch M.J., Trucks G.W., Schlegel H.B., Scuseria G.E., Robb M.A., Cheeseman J.R. (2009). Gaussian 09 revision C, 1. Gaussian Inc, Wallingford C.T.

[12] Stewart, J. J. (1989). Optimization of parameters for semi empirical methods II. Applications. *J. Comput. Chem.*, *10*(2), 221–264.

[13] Parr, R. G., Yang, W. (1989). *Density-functional Theory of Atoms and Molecules*, Oxford University Press, New York, Oxford.

[14] Khan, M. F., Rashid, R. B., Rahman, M. M., Al Faruk, M., Rahman, M. M., Rashid, M. A. (2017). Effects of solvent polarity on solvation free energy, dipole moment, polarizability, hyperpolarizability and molecular reactivity of aspirin. *Int. J. Pharm. Pharm. Sci, 9*(2), 217–221. doi: 10.22159/ijpps.2017v9i2.15853

[15] Vijayakumar, S., Kolandaivel, P. (2006). Study of static dipole polarizabilities, dipole moments, and chemical hardness for linear CH_3–(CC) n–X (X= H, F, Cl, Br, and NO_2 and n= 1–4) molecules. *J. Mol. Struct. THEOCHEM. 770*(1-3), 23–30. https://doi.org/10.1016/j.theochem.2006.04.030

[16] Afzal, Q. Q., Jaffar, K., Ans, M., Rafique, J., Iqbal, J., Shehzad, R. A., Mahr, M. S. (2022). Designing benzothiadiazole based highly efficient non-fullerene acceptor molecules for organic solar cells. *Polymer*, *238*, 124405. https://doi.org/10.1016/j.polymer.2021.124405

[17] Politzer, P.; Murray, J. S. (2004). *Molecular Electrostatic Potentials*; Taylor & Francis Group, LLC: New York, NY, USA.

[18] Mathammal, R.; Sangeetha, K.; Sangeetha, M.; Mekala, R.; Gadheeja, S. (2016). Molecular structure, vibrational, UV, NMR, HOMOLUMO MEP, NLO, NBO analysis of 3, 5 di tert butyl 4 hydroxy benzoic acid. *J. Mol. Struct., 1120*, 1–14. https://doi.org/10.1016/j.molstruc.2016.05.008

[19] Boufas, W.; Dupont, N.; Berredjem, M.; Berrezag, K.; Becheker, I.; Berredjem, H.; Aouf, N.-E. (2014). Synthesis and antibacterial activity of sulfonamides. SAR and DFT studies. *J. Mol. Struct.*, 1074, 180–185. https://doi.org/10.1016/j.molstruc.2014.05.066

[20] Ebenso, E. E., Arslan, T., Kandemirlı, F., Love, I., Öğretır, C., Saracoğlu, M., & Umoren, S. A. (2010). Theoretical studies of some sulphonamides as corrosion inhibitors for mild steel in acidic medium. *Int. J. Quantum. Chem.*, *110*(14), 2614–2636.

[21] Rezania, J., Behzadi, H., Shockravi, A., Ehsani, M., Akbarzadeh, E. (2018) Synthesis and DFT calculations of some 2-aminothiazoles, *J. Mol. Struct, 1157*, 300–305.
[22] Pandey, U.; Srivastava, M.; Singh, R.; Yadav, R. (2014). DFT study of conformational and vibrational characteristics of 2-(2-hydroxyphenyl) benzothiazole molecule. Spectrochim. *Acta Part A*, 129, 61–73. https://doi.org/10.1016/j.molstruc.2017.12.072
[23] Saout, G. L., Fayon, F., Bessada, C., Simon, P., Blion, A., Vaills, Y. (2001) A multispectroscopic study of $PbO_xZnO_{0.6}$−$x(P_2O_5)_{0.4}$ glasses, *J. Non-Cryst. Solids,* 293–295, 657–662.
[24] Brow, R. K. (2000) Review: The structure of simple phosphate glasses, *J. Non-Cryst. Solids, 263*, 1–28. https://doi.org/10.1016/S0022-3093(99)00620-1
[25] Schwarz, J., Tichá, H., Tichýa, L., Mertens, R. (2004). Physical properties of PbO-ZnO-P_2O_5 glasses. I. Infrared and Raman spectra, *J. Optoelectron. Adv. Mater*., 6, 737–746.
[26] Guo, H. W., Wang, X. F., Gong, Y. X. (2010). Mixed alkali effect in xK_2O-(30-x)Na_2O-30P_2O_5-40ZnO glasses*, J. Non Cryst Solids*, *356*, 2109–2113. https://doi.org/10.1016/j.jnoncrysol.2010.07.060
[27] Ternane, R., Ferid, M., Guyot, Y. (2008). Spectroscopic properties of Yb3C in $NaYbP_2O_7$ diphosphate single crystals. *J. Alloys Comp., 464*, 327–331
[28] Mandlule, A., Döhler, F., van Wüllen, L., Kasuga, T., Brauer, D. S. (2014). Changes in structure and thermal properties with phosphate content of ternary calcium sodium phosphate glasses. *J. Non-Cryst. Solid, 392*, 31–38. https://doi.org/10.1016/j.jnoncrysol.2014.04.002
[29] Abid, M., Et-tabirou, M., Hafid M. (2001). Glass forming region, ionic conductivity and infrared spectroscopy of vitreous sodium lead mixed phosphates. *Mater. Res. Bull. 36*, 407–421.
[30] Betthet, P., Bretey, E., Berthon, J., d'Yvoire, F., Belkebir, A., Rulmont, A., Gilbert, B. (1994). Structure and ion transport properties of Na_2O-Ga_2O_3-P_2O_5 glasses. *Solid State Ion., 70*, 476–481. https://doi.org/10.1016/0167-2738(94)90357-3